EAGE

A17

Location Uncertainties in Passive Seismic Monitoring

L. Eisner (MicroSeismic Inc.), W. Heigl (Apache Corporation) & P.M. Duncan* (MicroSeismic Inc.)

SUMMARY

In this study we shall address the effects of the receiver geometry, arrival time uncertainty and velocity model errors on location uncertainties. The effect of the velocity model error will be limited to a consideration of homogeneous media, although heterogeneity may have as profound effect on location accuracy as receiver distribution. Although many different sensor distributions are conceivable, we will focus on those that are most commonly applied in practice to include a 2-D grid of receivers on the earth s surface and linear arrays of receivers in vertical boreholes.

Accurate locations of induced seismic events in oil and gas reservoirs may provide important insight into reservoir geomechanics, describe fracture geometry and contribute to efficient reservoir exploitation. However, uncertainties of these locations are frequently neglected and false trends in located events are misinterpreted as results of geomechanical processes, although they have resulted from poorly constrained inversion. In this paper we address the effects of the receiver geometry, arrival time uncertainty and velocity model errors on location uncertainties. The effects of the velocity model error are limited to a consideration of homogeneous media, although heterogeneity may have as profound effect on location accuracy as receiver distribution. Although many different sensor distributions are conceivable, we focus on those that are most commonly applied in practice: a 2-D grid of receivers on the earth's surface and linear arrays of receivers in vertical boreholes.

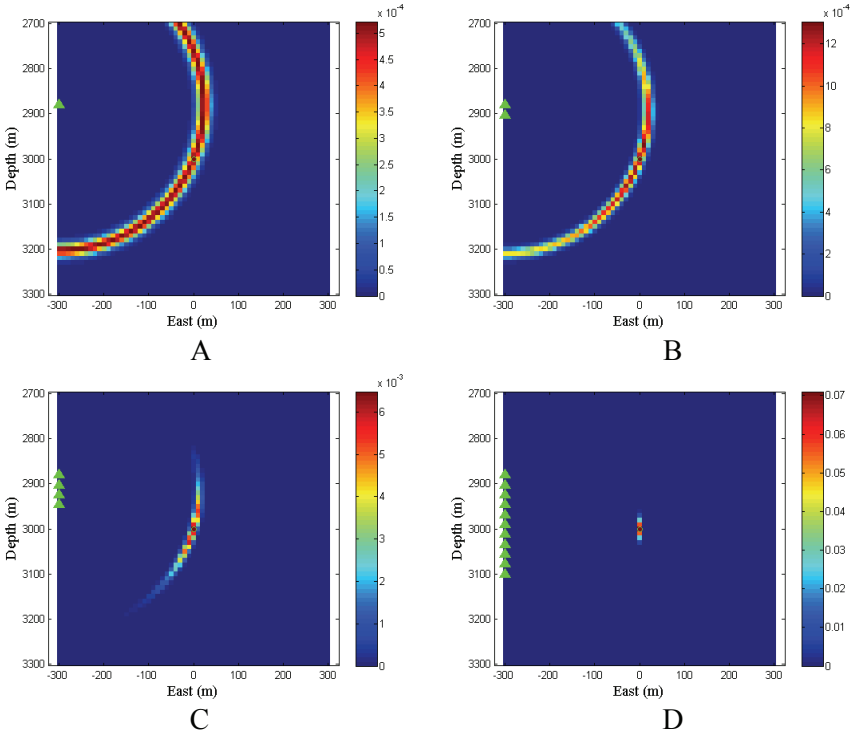

Figure 1. Vertical cross-sections though probability density functions (PDF) from 1 (plot A), 2 (B), 4 (C), and 11 (D) receivers in a single borehole and a microseismic event hypocenter located at the center of each plot (green circle). Hot colors show the most likely position of the located hypocenter. Decay from the hot to cold colors represents resolution and is determined by the acquisition geometry and the accuracy of the arrival times (assumed to be 1 ms). Each plot is normalized so that the probability density function sums to 1. The receivers are represented by green triangles on left side of each plot. Receiver spacing is 24 m and the maximum array spans 220 m vertically. P-wave and S-wave velocities are 5000 m/s and 3000 m/s, respectively.

Sources of microseismic event uncertainty

The commonly practiced surface and downhole location techniques work flawlessly for a homogeneous isotropic medium that is free of noise. In the real world, the wavefield propagating outward from a microseismic event is complex, raypaths are bent by velocity heterogeneities, and the particle polarization used to estimate azimuth may not be linear. In addition, varying levels of background noise may complicate the accurate picking of P- and S-wave arrival times, a factor that is especially significant for surface microseismic monitoring. For most surface and downhole projects, velocities for P- and S-waves are derived from sonic logs recorded in a nearby well. Among other things, sonic log measurements are hampered by near borehole effects, anisotropy, and bandwidth limitations

(sonic log bandwidth is usually more than an order of magnitude higher than seismic bandwidth). Downhole microseismic also requires the accurate measurement of event azimuth which in turn requires the accurate determination of the position and orientation of each receiver. Receiver position is calculated using a deviation survey, and receiver orientation is calculated with the use of calibration shots that are recorded when the borehole casing is perforated. Calibration to perforation shots is done under the assumption that the medium is laterally homogeneous and isotropic (or media with vertical axis of symmetry), and this assumption may also be a source of significant systematic error.

All these factors contribute to uncertainty in the estimated event location, but it is difficult to quantify exactly how each of them affects the final location. In this study, we focus on how acquisition geometry, picking error in varying noise environments, and velocity model error may affect the accuracy of microseismic event locations. To highlight these sources of error for both surface and downhole measurements, we calculate probability density functions of event locations that are derived from relevant arrival times and azimuthal measurements assuming Gaussian distributions of errors. When plotted in color, these probability density functions are a useful way to graphically illustrate the event location uncertainty and how it can be described in 3D space. To simulate picking error and velocity model misfit, we calculate probability density function from realizations of arrival times and azimuths that have been perturbed by Gaussian noise with zero mean and a chosen standard deviation.

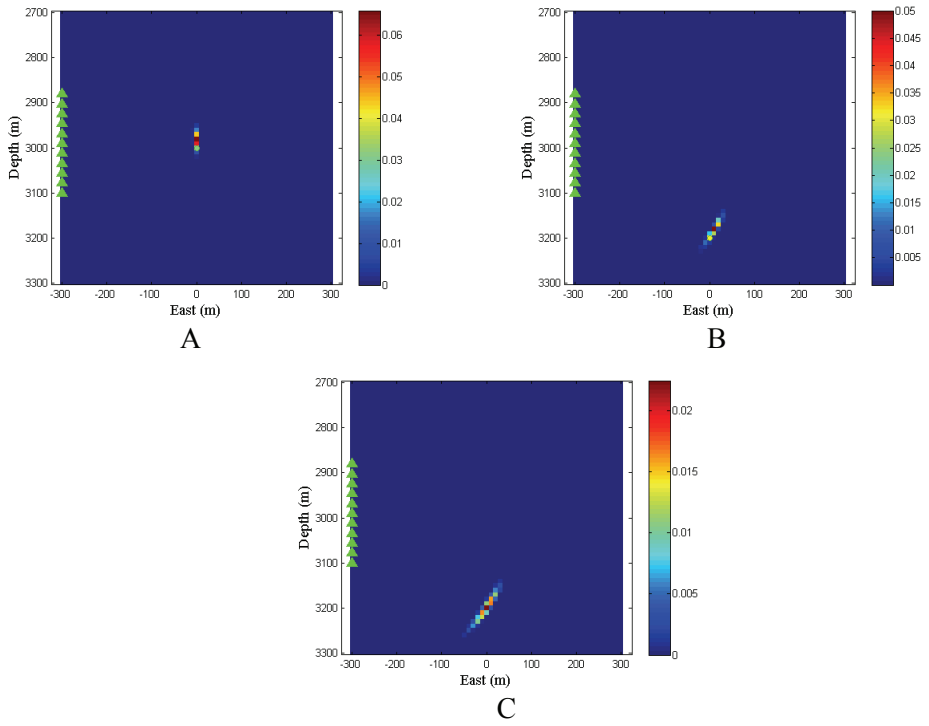

Figure 2. Vertical cross-sections though probability density functions (PDF) for events at various depths relative to the downhole receiver array. Plot A shows the PDF for a hypocenter located at a depth of the central receiver of the monitoring array. Plots B and C show the PDF for a hypocenter located below the borehole array (coordinates 0 and 3200 m). The arrival times of both P- and S-waves were perturbed with Gaussian random arrival time shifts of zero mean and 1 ms standard deviation. Plots A and B show one realization of this perturbation. Plot C shows an average PDF of 50 realizations of the Gaussian random arrival time shifts.

Downhole microseismic monitoring

A single receiver at which arrival times of P- and S-wave are measured constrains only the distance of the event from this receiver. Figure 1 illustrates how an array of geophones constrains depth and distance from a vertical well and was calculated with estimated pick uncertainty of 1 ms for arrival times of both P- and S-waves. In Figure 1, note that short arrays do not constrain the location very well. The location uncertainty is significantly reduced when receivers are located both above and below the event. Note that the resulting uncertainty in this cross-section from each array is largest in the vertical direction. This result is contrary to the common perception that depth is the best resolved coordinate from a vertical downhole array.

The shape of the event location uncertainty also depends on relative depth between the borehole array and the hypocenter. Figure 2 illustrates the shape of the uncertainty for two locations, one with a hypocenter depth directly in the center of the downhole receiver array (i.e., the same depth as in Figure 1) and one that is 80 m lower than the lowest receiver in the borehole array. Note that the probability density function of the deeper hypocenter is approximately twice as large and is tilted relative to the center of the array. To verify that this is not a result of a particular realization of the arrival time perturbation, we also show an average probability density function from 50 realizations of the arrival times and azimuths (Figure 2C). This averaged probability density function from 50 realizations shows a larger uncertainty compared to the 1 realization case. The tilted axis of the probability density function may cause systematic errors in event distributions for events located deeper than the downhole array. For example, a series of repeated deep events with similar hypocenters but various noise dependent arrival times would locate along the shape of the PDF and could be interpreted as a dipping fault.

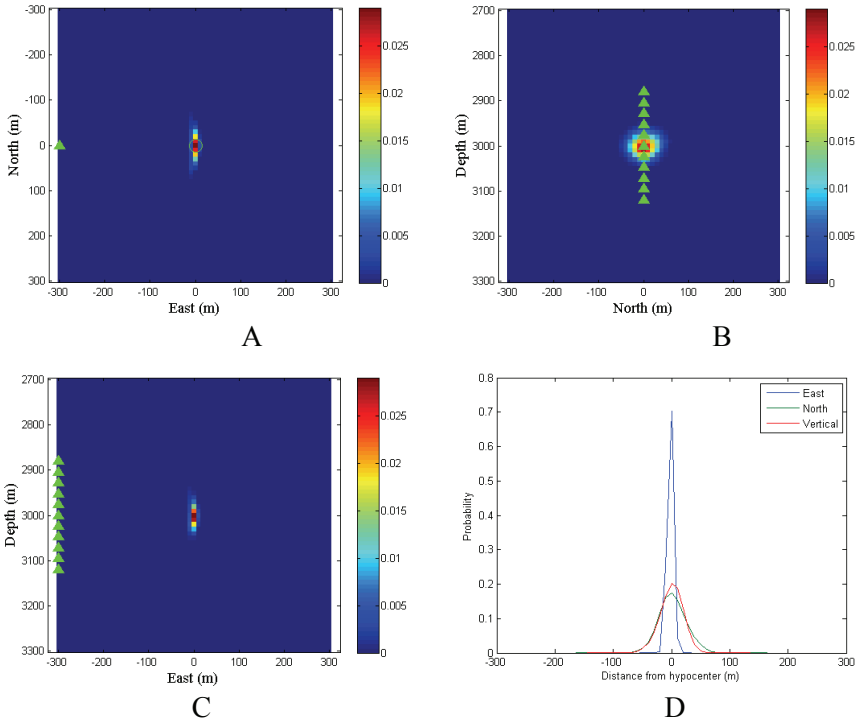

Figure 3. Three cross-sections through probability density functions of a hypocenter represented by the green circle located at East 0 m, North 0 m and depth 3000 m (3A - map view, 3B – N-S vertical cross-section, 3C – E-W vertical cross-section). 3D shows integrated 1-D marginal PDF's. The receivers are represented by green triangles. Plots show 50 realizations of traveltimes and backazimuth measurements perturbed with Gaussian perturbation of standard deviation of 1 ms and 10^{o}, respectively.

Figure 3 shows the true 3D uncertainty of a recorded microseismic event that includes lateral uncertainty resulting from particle polarization measurement. A Gaussian perturbation of azimuths with zero mean and a standard deviation of 10^o was used in this calculation. This standard deviation was selected based on a recently published study by Fischer et al. (2008) who showed that a standard deviation of 10^o and 15^o is reasonable for S-wave and P-wave derived backazimuths respectively. As shown in Figure 3, the event location is most tightly constrained in the radial direction away from the borehole location. Depth and azimuth are much more poorly constrained. The relative values of the radial, azimuthal, and depth uncertainties may be best viewed in the 1-D histogram in plot 4D. For an average of 50 realizations, we calculated uncertainties in Cartesian coordinates of 5 m in the East (radial) direction, 23 m in the North (azimuthal) direction, and 20 m in the vertical direction. It is important to note that the length of the downhole array is one of the major factors that control depth resolution.

Surface microseismic monitoring

Microseismic events are typically recorded at the surface using large arrays of vertical component geophones distributed on a 2-D grid. For our calculations, we assume a surface array of 121 receivers organized in an 11 by 11 square grid with 600 m receiver spacing. As with downhole acquisition, receiver density does not influence the probability density function of the located hypocenters assuming a reasonable density of receivers, however stacking of seismograms is essential for overcoming low signal-to-noise ratios. The probability density function is primarily constrained by the aperture of the array relative to the event depth. For our calculations, we locate 3000 m deep events monitored from a 6000 by 6000 m array.

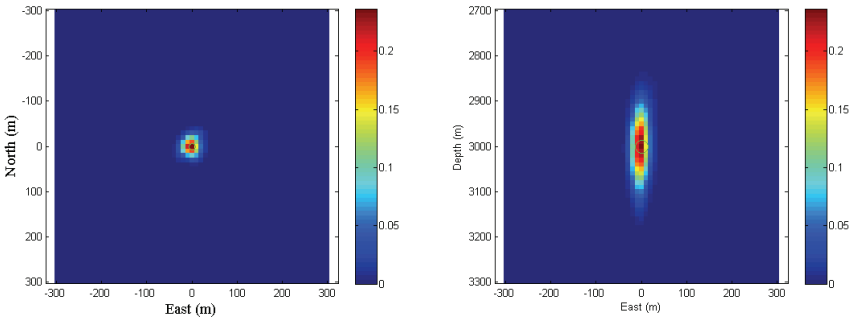

Figure 4. Two cross-sections through the 3-D probability density function of an event located at east and north 0 m and depth of 3000 m. The receiver array is an 11x11 square grid with 121 receivers. Event was located using only P-wave arrival times. P-wave arrival times were randomly perturbed with Gaussian distribution of zero mean and standard deviation of 10 ms. PDF represent an average of 45 realizations of these arrival times.

Figure 4 shows the probability density function of an event located using only P-wave arrival times recorded on the surface array. These arrival times were perturbed with Gaussian distribution of zero mean and standard deviation of 10 ms. The 10 ms uncertainty is considered as an upper bound and was derived from observed visible arrival times and their RMS. Recent datasets show an average RMS of 3.4ms with receiver statics derived from a string shot. Note that the horizontal uncertainty is relatively well constrained with standard deviations of 14 m and 15 m in east and north direction respectively. On the other hand, vertical uncertainty is relatively poorly constrained with a standard deviation of 58 m. However, if we use 4 ms uncertainty in traveltime uncertainty corresponding to the measured RMS residuals, like we did for downhole measurement, the vertical error is reduced to 25 m and less than 10 m in horizontal directions.

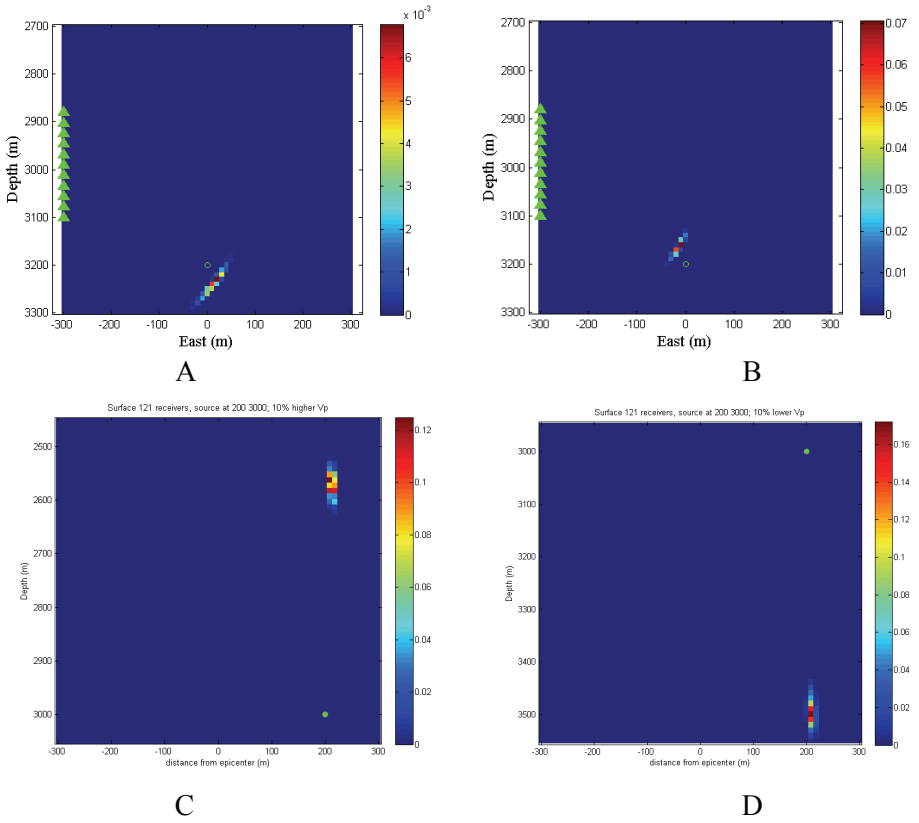

Figure 5: Four vertical cross-sections show velocity related location uncertainties for downhole monitoring (A and B) and surface monitoring (C and D). Plots A and C show a velocity model that is 10% faster and plots B and D show a velocity model that is 10% slower than the true velocity. All plots are shown at the same vertical and horizontal scale. For the downhole case, the arrival times were perturbed randomly with Gaussian distribution of zero mean and standard deviation of 1 ms for both P and S-waves. For the surface case, the arrival times were perturbed using a standard deviation of 4 ms for P-waves only. The true event location is represented with the green circle.

Event uncertainties resulting from velocity model errors

A significant source of location uncertainty originates from the unknown subsurface velocity structure between the source and receivers. The top two plots in Figure 5 illustrate a simple downhole case for which the P-wave and S-wave velocities have been increased by 10% (plot 5A) and decreased by 10% (plot 5B). Given the asymmetry of the borehole monitoring array relative to the hypocenter location, the location error due to the velocity model affects both the horizontal and vertical location proportionally to the velocity error, i.e. the distance from the array is increased by approximately 10%. Note that the slower velocity appears to have much smaller uncertainty, thus giving a false indication of higher accuracy.

For surface microseismic monitoring, perturbations of the velocity model have a minimal effect on horizontal event uncertainties. However, these same perturbations have a very significant effect on depth related event uncertainties (bottom two plots in Figure 5), again approximately proportional to the distance of the event from the monitoring array. For the fast velocity model, the event is incorrectly located at a shallow depth. The opposite is true for the slow velocity model. However, it is interesting to note that the horizontal position of the located event is minimally affected even though the event is not located at the center of the surface monitoring array. This vertical error is very effectively overcome through calibration of the velocity model with a perforation or check shot, analogous to the conventional seismic time-to-depth conversion.

Location uncertainties for dual downhole arrays

In this section, we investigate the uncertainty related to a single microseismic event that is detected on two vertical downhole arrays of 11 geophones separated by 600 m.

The top two plots in Figure 6 show the probability density function for an event located relatively close (30 m) to the plane of symmetry that connects the two monitoring wells. In this plot, the plane of symmetry is a horizontal line connecting the two wells in map view (top left plot in Figure 6). The bottom two plots in Figure 6 show the uncertainty related to an event that is relatively far away (200 m) from the plane of symmetry between the two wells. Intuitively, one might think that the most accurate locations would occur between the two wells. However, Figure 6 clearly illustrates that the location close to the plane of symmetry between the wells is more poorly constrained than the event farther away from the plane of symmetry.

Perhaps the most surprising result is shown in the right two plots which highlight the vertical uncertainty for the two events. The event far away from the plane of symmetry is much better constrained vertically than the event close to the plane of symmetry. In practice, linear clusters of event locations are often observed perpendicular to the plane of symmetry between dual monitoring wells. It is important to note that linear "trends" such as these may be geometrical artifacts that have nothing to do with fracture orientations.

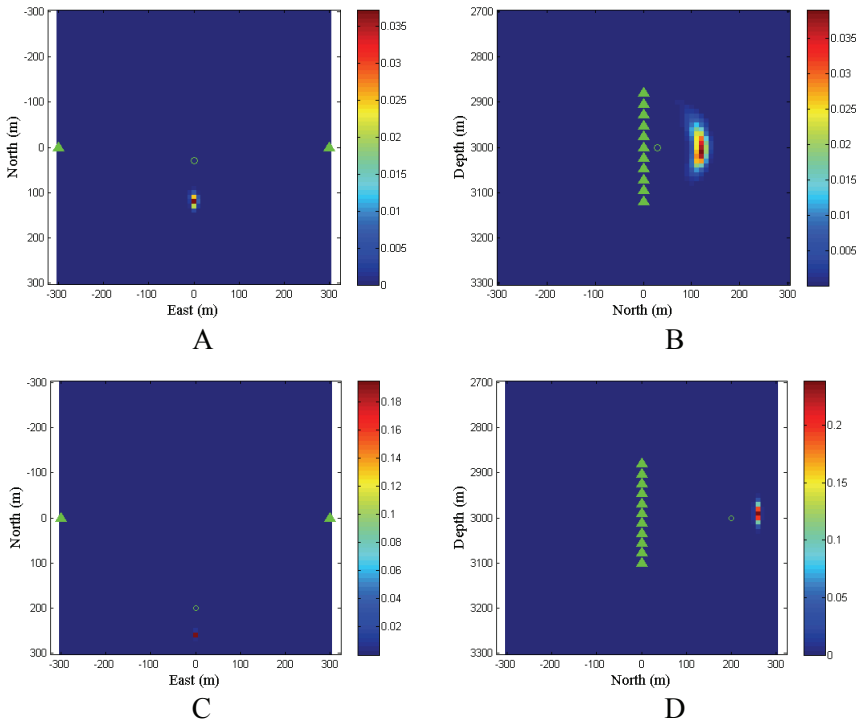

Figure 6: Dual borehole monitoring with incorrect (high) velocity model. Plots A and C show 2 map views at true hypocenter depths for locations derived from two monitoring vertical boreholes with 11 receivers each represented by the green triangles. Plots B and D show two vertical cross-sections through the true hypocenter (projected receiver positions are again represented by the green triangles). The true source position is represented by the green circle in each plot. Arrival times and backazimuths were perturbed randomly with Gaussian distribution of zero mean and standard deviation of 1 ms of both P and S-waves and 10^{o}, respectively and the probability density functions represent an average of 50 realizations of these perturbations.

Discussion

In this study, we have highlighted several common sources of error related to the location of microseismic events using both surface and downhole arrays. For downhole microseismic monitoring, the most accurate event locations are obtained when the depth of the located event occurs within the depth range of the monitoring array with an aperture comparable to the event distance (Figures 1 and 2). Contrary to common perception, we show that the depth of microseismic events recorded on a downhole array is much more poorly constrained than the radial distance from the borehole (Figures 1 and 3) assuming a correct inversion model. In addition, we illustrated in Figures 2b and 2c that uncertainties for events located deeper than the downhole array are smeared along an inclined trend that may easily be misinterpreted as fault or fracture planes.

Geophysicists typically think of velocity errors in terms of their affect on depth estimations. In Figures 5a and 5b, we illustrate how errors in the velocity model for downhole monitoring have the potential to cause both vertical and horizontal location errors. For dual downhole monitoring arrays (frequently encountered in reservoir monitoring), we show that event locations may be located preferentially in the direction perpendicular to the axis of symmetry between the monitoring wells (Figure 6). Again, these roughly linear event groupings may be incorrectly interpreted as induced fracture orientations to the untrained eye.

Event uncertainties for surface microseismic monitoring are significant but tend to be well behaved and easily interpreted in comparison to their downhole counterparts. Because of the noisy surface environment associated with reservoir production or fracture stimulation treatments, uncertainties related to traveltime picks are a significant source of error for events recorded on a surface array. These errors are partially mitigated through the use of a large, redundant array with thousands of receivers. As shown in Figure 4, location uncertainties for microseismic events recorded on a surface array are much more poorly constrained vertically than horizontally. As a general rule, depth estimation from a surface array is not as robust as from a downhole array. This fact becomes particularly apparent when considering depth location errors due to velocity model inaccuracies (Figures 6c and 6d). These sizable velocity related depth errors illustrate the need to carefully calibrate the velocity model using perforation shots early on in the surface microseismic processing workflow. It follows that if the main purpose of a microseismic experiment is to determine the vertical growth pattern of seismicity induced by hydrocarbon production or during hydraulic fracture stimulation, it may be prudent to use the downhole methodology if possible. However, a significant upside to the surface microseismic methodology is that the lateral location errors are very robust in comparison to downhole techniques. Surface microseismic event distributions are typically void of many of the systematic geometry induced errors inherent with downhole measurements. If determination of fracture orientation or azimuth in map view is the main objective of a particular microseismic experiment, the surface methodology may be a superior choice. In general, fewer interpretation pitfalls exist for surface microseismic and event distribution in map view is very stable even in light of the possibility of significant velocity and depth related errors.